Access to this work was provided by the University of Maryland, Baltimore County (UMBC) ScholarWorks@UMBC digital repository on the Maryland Shared Open Access (MD-SOAR) platform.

Please provide feedback

Please support the ScholarWorks@UMBC repository by emailing scholarworks-group@umbc.edu and telling us what having access to this work means to you and why it's important to you. Thank you.

PROCEEDINGS OF SPIE

SPIEDigitalLibrary.org/conference-proceedings-of-spie

A compressed sensing approach to hyperspectral classification

C. J. Della Porta, Bernard Lampe, Adam Bekit, Chein-I Chang

C. J. Della Porta, Bernard Lampe, Adam Bekit, Chein-I Chang, "A compressed sensing approach to hyperspectral classification," Proc. SPIE 10989, Big Data: Learning, Analytics, and Applications, 1098908 (13 May 2019); doi: 10.1117/12.2518382

SPIE.

Event: SPIE Defense + Commercial Sensing, 2019, Baltimore, Maryland, United States

Downloaded From: https://www.spiedigitallibrary.org/conference-proceedings-of-spie on 03 Oct 2019 Terms of Use: https://www.spiedigitallibrary.org/terms-of-use

A Compressed Sensing Approach to Hyperspectral Classification

C. J. Della Porta, Bernard Lampe, Adam Bekit, and Chein-I Chang
Remote Sensing Signal and Image Processing Laboratory, Department of Computer Science and Electrical Engineering, University of Maryland Baltimore County (UMBC), Baltimore, MD 21250

ABSTRACT

Although hyperspectral technology has continued to improve over the years, its use is often still limited due to size, weight and power (SWaP) constraints. One of the more taxing requirements, is the need to sample a large number of very fine spectral bands. The prohibitively large size of hyperpsectral data creates challenges in both archival and processing. Compressive sensing is an enabling technology for reducing the overall processing and SWaP requirements. This paper explores the viability of performing classification on sparsely sampled hyperspectral data without the need of performing sparse reconstruction. In particular, a spatial-spectral classifier based on a Support Vector Machine (SVM) and edge-preserving filters (EPFs) is applied directly in the compressed domain. The well-known Restricted Isometry Property (RIP) and a random spectral sampling strategy are used to evaluate analytically, the error between the compressed classifier and the full band classifier. The mathematical analysis presented shows that the classification error can be expressed in terms of the Restricted Isometry Constant (RIC) and that it is indeed possible to achieve full classification performance in the compressed domain, given that sufficient sampling conditions are met. A set of experiments are performed to empirically demonstrate compressed classification. Images from both the Airborne Visible / Infrared Imaging Spectrometer (AVIRIS) and Reflective Optics System Imaging Spectrometer (ROSIS) are examined to draw inferences on the impact of scene complexity. The results presented clearly demonstrate the possibility of compressed classification and lead to several open research questions to be addressed in future work.

Keywords: compressive sensing hyperspectral classification, support vector machines

1. INTRODUCTION

Hyperspectral sensing technologies have found success in a variety of applications such as agricultural surveys, land use mapping, food inspection, medical imaging and surveillance. Although hyperspectral technology has continued to improve over the years, its use is often still limited due to size, weight and power (SWaP) constraints. One of the more taxing requirements, is the need to sample a large number of very fine spectral bands. The high band count requires very fast and expensive analog-to-digital converters (ADCs), high capacity on-board storage and optimized computational hardware and software to allow for real-time processing. Such requirements limit the utility of many applications, and preclude the use of hyperspectral technologies in some application spaces entirely.

Compressive sensing techniques offer the potential of reducing the burdens imposed by the required sample rates. However, to fully exploit these benefits, hyperspectral algorithms must be applied directly in the compressed domain and ideally without an appreciable loss of performance. In this paper, the task of hyperspectral classification in the compressed domain is specifically considered. Two major contributions are made. First, error expressions between the full and compressed domains are derived for the linear support vector machine. This error expression shows, analytically, that full performance is indeed achievable in the compressed domain for sufficient sampling conditions. Second, a series of experiments are performed to demonstrate compressed classification of hyperspectral datasets. The experiments include two images of varying scenes from different sensors, and illustrate the effects of scene complexity.

Big Data: Learning, Analytics, and Applications, edited by Fauzia Ahmad,
Proc. of SPIE Vol. 10989, 1098908 · © 2019 SPIE · CCC code:
0277-786X/19/$18 · doi: 10.1117/12.2518382

Downloaded From: https://www.spiedigitallibrary.org/conference-proceedings-of-spie on 03 Oct 2019
Terms of Use: https://www.spiedigitallibrary.org/terms-of-use

2. SPARSE HYPERSPECTRAL SAMPLING

Compressive sensing (CS), or sparse sampling, is a sensing paradigm that, under the right circumstances, is able to recover signals of interest at sub-Nyquist sample rates, using non-adaptive strategies. As the name implies, compressive sensing is the process of acquiring information in an already compressed state. The full signal can later be uncompressed, or recovered, using one of many sparse recovery algorithms.

2.1 Compressive Sensing Framework

The sparse sampling process, for an $L \times 1$ signal of interest $\boldsymbol{r}$ and an $m \times 1$ sparsely sampled signal $\boldsymbol{y}$, can be defined mathematically as shown in (1).

$$\boldsymbol{y} = \boldsymbol{\Phi}\,\boldsymbol{\Psi}\boldsymbol{r} + \boldsymbol{n} \tag{1}$$

In this equation, $\boldsymbol{\Psi}$ is an $L \times L$ sparsifying transformation matrix, $\boldsymbol{\Phi}$ is an $m \times L$ sampling matrix and $\boldsymbol{n}$ is an $m \times 1$ error vector. Such sampling strategies depend on two key principles: sparsity and incoherence [1]. The signal of interest, $\boldsymbol{r}$, must be sparse when expressed in the appropriate basis, $\boldsymbol{\Psi}$, and must be sampled in a basis, $\boldsymbol{\Phi}$, that is maximally incoherent with the representation basis.

Contrary to dimensionality reduction methods, such as Principal Component Analysis (PCA) [2], compressive sensing strategies must be implemented without knowledge of the full signal and, therefore, rely on probabilistic convergence guaranteed under specific conditions. The restricted isometry property (RIP) [1] is a very important property that is typically imposed in CS to guarantee that relative measures of distance are maintained between the original and compressed signal domains. The RIP, for a signal $\boldsymbol{r}$, with sparsity level k, is defined mathematically as shown in (2).

$$(1 - \delta_k)\|\boldsymbol{r}\|_2^2 \leq \|\boldsymbol{\Phi}\boldsymbol{r}\|_2^2 \leq (1 + \delta_k)\|\boldsymbol{r}\|_2^2 \tag{2}$$

Here, δ_k, defined as the restricted isometry constant (RIC), is the smallest possible constant that satisfies the equation for all k-sparse vectors in $\boldsymbol{r}$. As the dimensionality of the sparse vector, m, approaches the dimensionality of the original signal, L, the RIC approaches zero resulting in an exact preservation of lengths.

2.2 Compressive Sensing of Hyperspectral Pixel Vectors

One the most difficult challenges in designing a compressive sensing system is to identify the domain in which the signal of interest is optimally sparse. Previous works have suggested the use of the discrete cosine transform (DCT) [3], wavelet transforms [4], and dictionary learning approaches [5]. Fortunately, knowledge of the sparsifying basis is only required for the reconstruction process and can be ignored for compressed algorithms [6]. The simplified model, shown in (3), can be adopted, based on a random sampling strategy and the utility of universality [7].

$$\boldsymbol{y} = \boldsymbol{\Phi}_{\mathcal{N}}\boldsymbol{r} \tag{3}$$

The sampling matrix can be constructed from any distribution that satisfies the concentration measure of inequalities [7]. For this family of sampling matrices, it can be shown, with overwhelming probability, that RIP is satisfied given that

$$m \geq C \cdot k \log(L/k) \tag{4}$$

Downloaded From: https://www.spiedigitallibrary.org/conference-proceedings-of-spie on 03 Oct 2019
Terms of Use: https://www.spiedigitallibrary.org/terms-of-use

where C is a constant that depends on each particular instance. For this work, the Gaussian distribution is specifically chosen, where each element is distributed as $\phi_{ij} \sim N(0,1/L)$ and the columns are normalized to unit length.

3. HYPERSPECTRAL CLASSIFICATION

Classification is one of the many tasks performed on hyperspectral images. The spectral diversity intrinsically available in hyperspectral data can be leveraged directly as classification features. Hyperspectral classification continues to be a very active area of research utilizing state-of-the-art classifiers, such as deep neural network architectures [8][9][10], kernel-based discriminators [11][12], statistical learning theory [13], and complex feature strategies based on both spatial and spectral features [14][15][16]. For this work a joint spectral-spatial classifier based on a support vector machine and edge preserving filters is employed to demonstrate classification in the compressed domain.

3.1 Linear Support Vector Machines

The support vector machine (SVM) [17] is a popular classifier that has been successfully applied in hyperspectral applications and is well understood in the machine learning and pattern recognition communities. The SVM is a binary discriminant function that defines an L-dimensional hyperplane separating two classes described by L features. The linear SVM can be defined as the discriminant function shown in (5), where the weight vector $\boldsymbol{\omega}$ bias b are maximized using a maximum margin objective function, subject to $||\boldsymbol{\omega}|| = 1$. A hard classification of unknown inputs is performed by observing the sign of the output, where positive values belong to one class and negative values belong to the other. Although, the SVM is natively a binary classifier, it is often extended to multinomial classification problems through the use of a binary extension strategy, such as one-vs-rest or one-vs-one.

$$f(\boldsymbol{r}) = \boldsymbol{\omega}^T \boldsymbol{r} + b \tag{5}$$

To make SVMs more mathematically convenient, the *Representer Theorem* [18] is often leveraged. The theorem states that, with appropriate constraints, $\boldsymbol{\omega}$ can always be written as a linear combination of the training data, $\boldsymbol{\omega} = \sum_{j=1}^{N} \alpha_j d_j \boldsymbol{r}_j^T$, where $d_j \in \{-1,1\}$ is the training label, $\alpha_j \in [0,1]$ is a linear coefficient and N is the total number of training samples. Substituting this relationship, the linear SVM discriminant function can also be written as shown in (6), where the bias term is implicitly included in the weight vector. In general, most values of α_j will be zero and the non-zero values are referred to as the support vectors. In this form, the SVM is completely described by the choice of the support vectors, which are typically solved for iteratively.

$$f(\boldsymbol{r}) = \sum_{j=1}^{N} \alpha_j d_j \boldsymbol{r}_j^T \boldsymbol{r} \tag{6}$$

Classification in the compressed domain can be represented using a modification of the discriminant function that includes the sparse acquisition matrix. The compressed discriminant function then takes the form shown in (7), where the subscript s, for α, denotes the fact that the SVM in the compressed domain is not guaranteed to use the same support vectors or bias.

$$f_s(\boldsymbol{r}) = \sum_{j=1}^{N} \alpha_{s_j} d_j \left(\boldsymbol{\Phi r}_j\right)^{\mathbf{T}} \boldsymbol{\Phi r} \tag{7}$$

To examine the performance of the support vector in the classified domain, an error function can be constructed between the original and compressed domains. Let $\epsilon = |f(\boldsymbol{r}) - f_s(\boldsymbol{\Phi r})|$ denote the absolute error between the fully sampled and the sparsely sampled classifiers.

Downloaded From: https://www.spiedigitallibrary.org/conference-proceedings-of-spie on 03 Oct 2019
Terms of Use: https://www.spiedigitallibrary.org/terms-of-use

$$\epsilon = \left| \sum_{j=1}^{N} \alpha_j d_j \boldsymbol{r}_j^T \boldsymbol{r} - \sum_{j=1}^{N} \alpha_{s_j} d_j \left(\boldsymbol{\Phi} \boldsymbol{r}_j\right)^{\mathrm{T}} \boldsymbol{\Phi} \boldsymbol{r} \right| \tag{8}$$

In general, it is impossible to derive a closed form solution for this expression since the support vectors are solved iteratively in practice. Additionally, there is no guarantee of a unique solution when solving for these model parameters. To simplify the analysis, the support vectors are chosen, without guarantee of optimality, to be the same in the sparsely sampled domain. This implies that $\alpha_{s_j} = \alpha_j, \forall\, j$, reducing the error function as shown in (9).

$$\epsilon = \left| \sum_{j=1}^{N} \alpha_j d_j \left[\boldsymbol{r}_j^T \boldsymbol{r} - \left(\boldsymbol{\Phi} \boldsymbol{r}_j\right)^{\mathrm{T}} \boldsymbol{\Phi} \boldsymbol{r} \right] \right| \tag{9}$$

Furthermore recognizing that $\boldsymbol{r}_j^T \boldsymbol{r} = \left\| \boldsymbol{r}_j \right\|_2^2$, the classification error can be defined as:

$$\epsilon = \left| \sum_{j=1}^{N} \alpha_j d_j \left(\left\| \boldsymbol{r}_j \right\|_2^2 - \left\| \boldsymbol{\Phi} \boldsymbol{r}_j \right\|_2^2 \right) \right| \tag{10}$$

Given that the sampling matrix, $\boldsymbol{\Phi}$, satisfies the RIP in equation (2), the error can be re-written as an inequality in terms of the RIC, δ_k, as

$$\epsilon \leq \left| \sum_{j=1}^{N} \alpha_j d_j \left(\left\| \boldsymbol{r}_j \right\|_2^2 - (1 - \delta_k) \left\| \boldsymbol{r}_j \right\|_2^2 \right) \right| \tag{11}$$

Expanding the RIC term and simplifying, the final error can be written as

$$\epsilon \leq \left| \sum_{j=1}^{N} \alpha_j d_j \left\| \boldsymbol{r}_j \right\|_2^2 \delta_k \right| \tag{12}$$

It follows that the classification error is directly bounded by the RIC and will go to zero for all m that satisfy the condition shown in (4), as δ_k goes to zero. This derivation demonstrates that it is indeed possible to approach full classification performance in the compressed domain, for sufficient sampling conditions.

3.2 Edge Preserving Filters

Spatial correlation between neighboring pixels must be taken into to achieve state-of-the-art hyperspectral classification performance. To provide the aid of special context, guided edge-preserving filters (EPF) are applied to the classifier [16]. In this approach, the spatial-spectral classification process is treated as a probability optimization problem. The initial pixel class probabilities are determined by a spectral only classifier, such as the support vector machine in this case, and then refined by an edge-preserving filtering process. Specifically, the guided EPF filter based on a 3 channel principal component image, as described in [16], has been used for all experiments. A description of the full classification algorithm is shown in Table 1.

Downloaded From: https://www.spiedigitallibrary.org/conference-proceedings-of-spie on 03 Oct 2019
Terms of Use: https://www.spiedigitallibrary.org/terms-of-use

Table 1. Edge Preserving Filter Classification Algorithm

Edge Preserving Filter Classification Algorithm

Input: A hyperspectral image $R \in \Re^{N_x \times N_y \times L}$

1. Generate a classification map, $C_{SVM} \in \Re^{N_x \times N_y}$, using any pixelwise classifier.
2. Generate an initial binary probability map, $P_{i,l} \in [0,1]$, by assigning the pixelwise class to each respective channel as $P_{i,l} = \begin{cases} 1, & if\ c_i = l \\ 0, & otherwise \end{cases}$
3. Optimize the probability map by applying an edge preserving filter, $\acute{P}_{i,n} = \sum_j W_{i,j}(I) P_{i,n}$, where the weights, $W_{i,j}$, depend on the choice of EPF and the guidance image I.
4. Generate the final classification map by choosing the class with the highest probability $C_{EPF} = arg \max_{1 \le n \le P} \acute{P}_{i,n}$

Output: A final classification map, $C_{EPF} \in \Re^{N_x \times N_y}$

4. EXPERIMENT

Simulated experiments were performed comparing the accuracy of the support vector machine on fully sampled and sparsely sampled hyperspectral data. Two images were used in total; one scene was selected from the Airborne Visible / Infrared Imaging Spectrometer (AVIRIS) [19] and one scene was selected from the Reflective Optics System Imaging Spectrometer (ROSIS) [20]. The AVIRIS is an aircraft-based hyperspectral sensor with 224 contiguous bands over the 400-2500 nm spectrum with 10 nm spectral resolution. The selected AVIRIS image was collected over Purdue's Indiana Indian Pines test site and is composed of a mixture of agriculture and forestry with 20m spatial resolution [21]. It is a well-known benchmark dataset for hyperspectral classification and consists of 200 spectral channels after removal of the water absorption bands. The provided ground truth includes 16 classes and background (BKG) samples as shown in Figure 1.

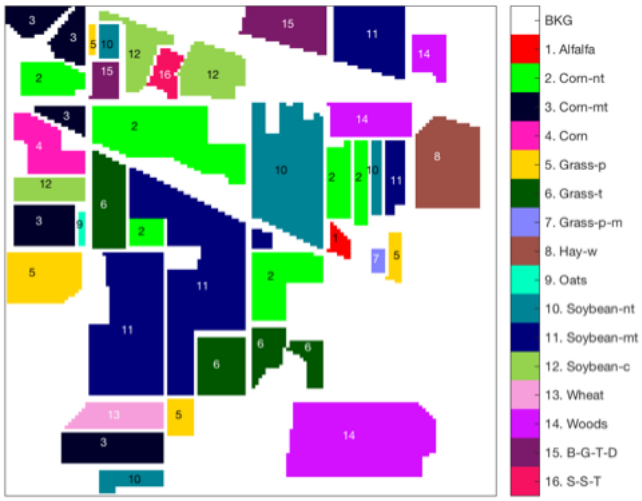

Figure 1. Indian Pines ground truth image.

ROSIS is an aircraft based hyperspectral sensor with 115 contiguous bands over the 430-860 nm spectrum with a spatial resolution of 1.3-meter per pixel and spectral resolution of 4 nm (12 most noisy channels were removed before experiments). The sensor was originally designed for resolving fine spectral structures and has produced several images that have been widely used within the literature. One ROSIS image was used for the experiments, the Pavia University image scene [22] which is another well-known benchmark dataset for hyperspectral classification. The image has 1.3m

Downloaded From: https://www.spiedigitallibrary.org/conference-proceedings-of-spie on 03 Oct 2019
Terms of Use: https://www.spiedigitallibrary.org/terms-of-use

spatial resolution and consists of 102 spectral channels after removal of the water absorption bands. The image was collected over Pavia, northern Italy and is composed of urban scenes. The provided ground truth consists of 9 different classes and is shown in Figure 2.

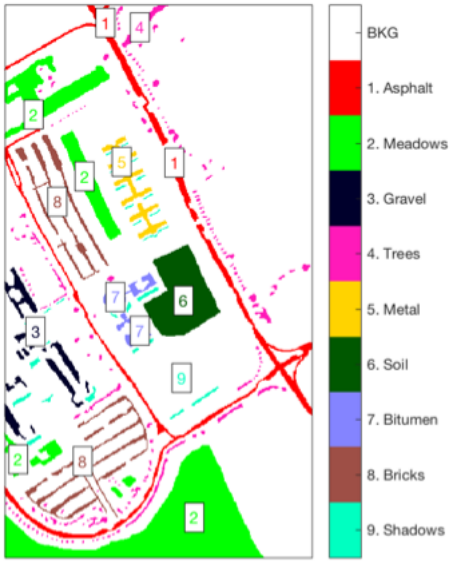

Figure 2. Pavia University ground truth image.

4.1 Experimental Setup

The sparse hyperspectral pixel vectors were modelled using random Gaussian sensing matrices with m samples taken. The number of compressed bands, m, was varied from five up to the full band number of bands for each image. Additionally, the sampling noise, $\boldsymbol{n}$, has been omitted for simplicity. The RBF-based SVM was used as the spectral classifier, with the tuneable kernel parameter set to 0.72 and 0.64 for Indian Pines and Pavia University, respectively. The analytic proof of convergence for the RBF kernel SVM is left for future work. The edge preserving filtering process was based on a guided filter with a color guidance image, based on the first 3 principal components, i.e., EPF-G-c.

For each experiment, the pixel vectors were randomly partitioned into training and test sets following the same set-up described in [16]. The exact number of training and test samples are tabulated in Table 2 and Table 3, for the Indian Pines and Pavia University images, respectively.

Table 2: Indian Pines training and test sample counts

Class Name	Training Samples	Test Samples	Class Name	Training Samples	Test Samples
Alfalfa	25	21	**Soybean-notil**	81	891
Corn-notil	83	1345	**Soybean-mintil**	99	2356
Corn-mintil	78	752	**Soybean-clean**	73	520
Corn	68	169	**Wheat**	70	135
Grass-pasture	79	404	**Woods**	90	1175
Grass-trees	78	652	**Building**	65	321
Grass-mowed	14	14	**Towers**	46	47

Downloaded From: https://www.spiedigitallibrary.org/conference-proceedings-of-spie on 03 Oct 2019
Terms of Use: https://www.spiedigitallibrary.org/terms-of-use

Hay-windrow	66	412	**BKG**	0	10,076
Oates	10	10			

Table 3: Pavia University training and test sample counts.

Class Name	Training Samples	Test Samples	Class Name	Training Samples	Test Samples
Asphalt	286	6345	**Bare Soil**	285	4744
Meadow	286	18363	**Bitumen**	285	1045
Gravel	285	1814	**Bricks**	285	3397
Trees	285	2779	**Shadows**	285	662
Metal	285	1060	**BKG**	0	164,624

4.2 Classification Accuracy in the Compressed Domain

Classification accuracy was selected as the primary performance metric. The individual class accuracy is defined as shown in equation (13). In this form, M represents the total number of classes and n_{ij} represents the number of samples in the *i*th class that have been classified in the *j*th class. To reduce this down to a single metric, the average accuracy (AA) is defined as shown in equation (14). Finally, the overall accuracy (OA) is an additional summary metric that is defined as shown in equation (15).

$$P_A(C_i) = \frac{n_{ii}}{\sum_{j=1}^{M} n_{ji}} \tag{13}$$

$$\mathrm{P_{AA}} = \frac{1}{M}\sum_{i=1}^{M} P_A(C_i) \tag{14}$$

$$P_{OA} = \frac{1}{N}\sum_{i=1}^{M} n_{ii} \tag{15}$$

P_{OA} and P_{AA} are calculated for both images and plotted in Figure 3 versus m-compressively sensed bands (CSBs) with m ranging from 1 to 220 where the plots had a large jump around 30 CSBs, and then began flat after 100 CSBs with near full band performance. As can be seen in the figure the maximum performance was achieved using approximately 50% of the total number of CSBs. The range of accuracy for this image is significant with just over a 20% difference in accuracy between the minimum number of CSBs and using full CSBs. This particular image has most imbalanced classes and was also the most difficult one among the four images that were tested. The presented results are in line with many of the performance measures reported in the literature. For the ROSIS image, both accuracies converged quickly between 20 and 40 CSBs. This ROSIS image showed a similar trend to the AVIRIS image. There is an exponential increase in performance for the lower number of CSBs. Similarly, the range of accuracy values between the fewest CSBs and the full band performance is quite significant with a total difference of about 15% for the overall accuracy and 20% for the average accuracy.

Downloaded From: https://www.spiedigitallibrary.org/conference-proceedings-of-spie on 03 Oct 2019
Terms of Use: https://www.spiedigitallibrary.org/terms-of-use

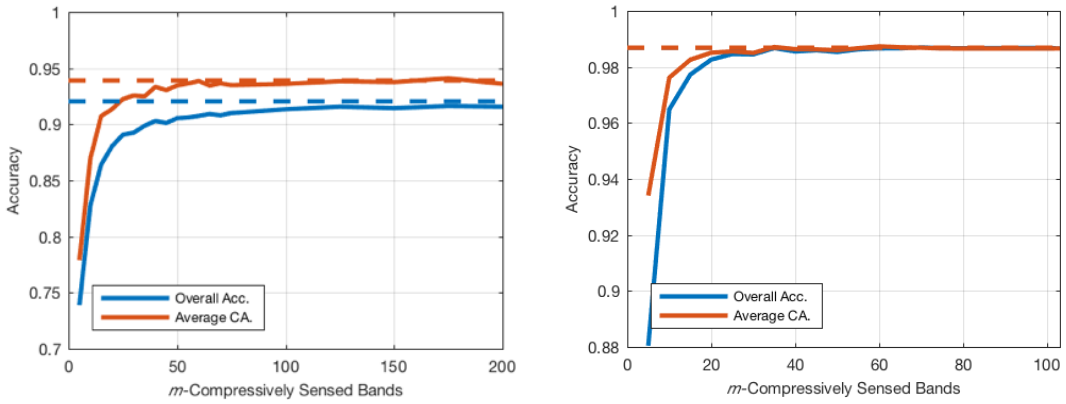

Figure 3. Classification accuracy results. Indian Pines (left) and Pavia University (right).

5. CONCLUSION

Hyperspectral classification in the compressed domain was explored in this work with the motivation of enabling low-cost, low-SWAP Hyperspectral designs. Error bounds were derived between the full band and compressed band classifier for the linear support vector machine. The derived bounds showed that full classification performance could be achieved in the compressed domain for a compressed system that satisfies the RIP condition.

Classification experiments were performed for two different hyperspectral sensors, AVIRIS and ROSIS. The experimental results demonstrated that, for sufficient amounts of sub-sampling, the classification performance of the fully sampled domain can be achieved in the sparsely sampled domain. The experiments also highlighted the fact that the intrinsic sparsity of the images varied, requiring differing levels of sub-sampling to achieve full classification accuracy. These results also point to the important question of choosing the sub-sampling level if they scene complexity is not known a priori, which will be addressed in future work.

REFERENCES

[1] Candes, E. J., and Wakin, M. B., "An Introduction to Compressive Sampling", IEEE Signal Processing Magazine 25(2), 21-30 (2008)
[2] Wold. S, Esbensen. K., and Geladi, P., "Principal Component Analysis", Chemometrics and Intelligent Laboratory Systems, 2(1-3), 37-52 (1987)
[3] Amhed, N., Natarajan, T., and Rao, K. R., "Discrete Cosine Transform", IEEE Transactions on Computers, 100(1), 90-93 (1974)
[4] Antonini, M., Barlaud, M., Mathieu, P., and Daubechies, I., "Image coding using wavelet transform", IEEE Transactions on image processing", 1(2), 205-220 (1992)
[5] Li, C., Ma, L., Wang, Q. Zhou, Y., and Wang, N., "Construction of Sparse Basis By Dictionary Training for Compressive Sensing Hyperspectral Imaging", IEEE International Geosicence and Remote Sensing Symposium (IGARSS), 1442-1445 (2013)
[6] Della Porta, C. J., Bekit, A., Lampe, B., and Chang, C-I, "A Universal Sensing Model for Compressed Hyperspectral Image Analysis", Proceedings of the SPIE 10986, Baltimore (2019)
[7] Baraniuk, R. G., Davenport, M. A., De Vore, R., and Wakin, M. B. "A Simple Proof of the Restricted Isometry Property for Random Matrices", Constructive Approximation 28(3), 253-263 (2008)
[8] Chen, Y., Lin, Z., Zhao, Z., Wang, G., and Gu, Y., "Deep Learning-Based Classification of Hyperspectral Data", IEEE Journal of Selected Topics in Applied Earth Observations and Remote Sensing", 7(6), 2094-2107 (2014)
[9] Li, T., Zhang, J. and Zhang, Y., "Classification of Hyperspectral Image Based on Deep Belief Networks", In IEEE Image Processing (ICIP), (2014)

Downloaded From: https://www.spiedigitallibrary.org/conference-proceedings-of-spie on 03 Oct 2019
Terms of Use: https://www.spiedigitallibrary.org/terms-of-use

[10] Chen, Y., Zhao, X., and Jia, X. "Spectral-spatial Classification of Hyperspectral Data Based on Deep Belief Network", IEEE Journal of Selected Topics in Applied Earth Observations and Remote Sensing, 8(6), 2381-2392 (2015)
[11] Camps-Valls G., and Bruzzone, L., "Kernel-based Methods for Hyperspectral Image Classification", IEEE Transactions on Geoscience and Remote Sensing, 43(6), 1351-1362 (2005)
[12] Camps-Valls, G., Gomez-Chova, L., Munoz-Mari, J., Vila-Frances, J., and Calpe-Maravilla, J., "Composite Kernels for Hyperspectral Image Classification", IEEE Geoscience and Remote Sensing Letters, 3(1), 93-97 (2006)
[13] Camps-Valls, G., Tuia, D., Bruzzone, L., and Benediktsson, J. A., "Advances in hyperspectral image classification: Earth monitoring with statistical learning methods", IEEE Signal Processing Magazine, 31(1), 45-54 (2014)
[14] Fauvel, M., Benediktsson, J. A., Chanussot, J., and Sveinsson, J. R., "Spectral and spatial classification of hyperspectral data using SVMs and morphological profiles", In 2007 IEEE International Geoscience and Remote Sensing Symposium, 4834-4837 (2008)
[15] Fauvel, M., Tarabalka, Y., Benediktsson, J. A., Chanussot, J., and Tilton, J. C., "Advances in spectral-spatial classification of hyperspectral images", Procedings of the IEEE, 101(3), 652-675 (2013)
[16] Kang, X., Li, S., and Benediktsson, J. A., "Spectral-spatial hyperspectral image classification with edge-preserving filtering", IEEE Transactions on Geoscience and Remote Sensing, 52(5), 2666-2677 (2014)
[17] Cortes, C. and Vapnik, V., "Support-Vector Machines", Machine Learning, 20, 273-297 (1995)
[18] Schokopf, B., Herbrich, R., and Smola, A. J., "A generalized representer theorem" In International Conference on Computational Learning Theory, Berlin (2001)
[19] Vane, G., Green, R. O., Chrien, T. G., Enmark, H. T., Hansen, E. G., and Porter, W. M., "The airborne visible/infrared imaging spectrometer (AVIRIS)", Remote sensing of environment, 44(2-3), 127-143 (1993)
[20] Gege, P. Beran, D., Mooshuber, W., Schulz, J., and Van Der Piepen, H., "System Analysis and Performances of the New Version of the Imaging Spectrometer ROSIS", in Proceedings of the First EARSel Workshop on Imaging Spectroscopy, (1998)
[21] Baumgardner, M. F., Biehl, L. L., and Landgrebe, D. A., "220 Band AVIRIS Hyperspectral Image Data Set: Jun 12, 1992 Indian Pines Test Site 3", Purdue University Research Repository, 2015
[22] "Universidad del Pais Vasco Grupo de Inteligencia Computacional", http://www.ehu.eus/ccwintco/index.php?title=Hyperspectral_Remote_Sensing_Scenes#Salinas (June 2018)

Downloaded From: https://www.spiedigitallibrary.org/conference-proceedings-of-spie on 03 Oct 2019
Terms of Use: https://www.spiedigitallibrary.org/terms-of-use